Numerical Investigation of Fluid and Thermal Flow in a Differentially Heated Side Enclosure Walls at Various Inclination Angles

C.S. Nor Azwadi[1] and N.I.N. Izual[2]

Abstract: Natural convection in a differentially heated enclosure plays vital role in engineering applications such as nuclear reactor, electronic cooling technologies, roof ventilation, etc. The developed thermal flow patterns induced by the density difference are expected to be critically dependence on the inclination angles of the cavity. Hence, thermal and fluid flow pattern inside a differentially heated side enclosure walls with various inclination angles have been investigated numerically using the mesoscale lattice Boltzmann scheme. Three different dimensionless Rayleigh numbers were used, and a dimensionless Prandtl number of 0.71 was set to simulate the circulation of air in the system. It was found that the number, size and shape of the vortices in the enclosure were significantly affected by the Rayleigh number and inclination angle of the enclosure. The plots of temperature lines and the average Nusselt number in the enclosure clearly depict the temperature distribution as a function of Rayleigh number and inclination angles.

Keywords: Double population, lattice Boltzmann, distribution function, BGK collision, natural convection.

1   Introduction

Flow and heat transfer analysis in an enclosure driven by buoyancy force is one of the most widely studied problems in thermo-fluid area. This type of flow can be found in certain engineering applications within electronic cooling technologies, in everyday situation such as roof ventilation or in academic research where it may be used as a benchmark problem for testing newly developed numerical methods. A classic example is the case where the flow is induced by differentially heated walls boundaries of a cavity. Two vertical walls with constant hot and cold temperature is the most well defined geometry and was studied extensively in the literature. A

---

[1] Faculty of Mechanical Engineering, Universiti Teknologi Malaysia, Malaysia
[2] Faculty of Mechanical Engineering, Universiti Malaysia Pahang, Malaysia

comprehensive review was presented by Said et. al (2005). Other examples are the work by Azwadi and Tanahashi (2006), Davis (1983) and Tric et. al (2000).

The analysis of flow and heat transfer in a differentially heated side walls was extended to the inclusion of enclosure's inclination to the direction of gravity by Rasoul and Prinos (1997). This study performed numerical investigations into two-dimensional thermal fluid flows which are induced by the buoyancy force when the two facing sides of the cavity are heated to different temperature. The cavity was inclined at angles from 40^0 to 60^0, Rayleigh numbers from 10^3 to 10^6 and Prandtl numbers from 0.02 to 4000. Their results indicated that the mean and local heat flux at the hot wall were significantly depended on the inclination angles. They also found that this dependence becomes stronger for inclination angles greater than 90^0.

Hart (1971) performed theoretical and experimental study of thermal fluid flow in a rectangular cavity at small aspect ratio and investigated the stability of the flow inside the system. Ozoe et. al (1974) conducted numerical analysis using finite difference method of two-dimensional natural circulation in four types of rectangular cavity at inclination angles from 0^0 to 180^0. Kuyper et. al (1993) provided a wide range of numerical predictions of flow in an inclined square cavity, covered from laminar to turbulent regions of the flow behavior. They applied k-ε turbulence model and performed detailed analysis for Rayleigh numbers of 10^6 to 10^{10}.

The effect of inclination angles on an air filled, differentially heated and adiabatic top and bottom boundaries of a square cavity was numerically investigated for three different Rayleigh numbers. This study enables us to determine the influences of inclination angle on the heat transfer mechanism and fluid flow behavior in the enclosure. In the present study, the incompressible, two-dimensional governing equations are solved indirectly, i.e. by using the lattice Boltzmann method with second order accuracy in space and time. The double distribution function type of thermal lattice Boltzmann model were proposed, where the fluid flow and thermal fields are solved using two different evolutions of particle distribution functions [Nor Azwadi and Tanahashi (2007); Guo et. al (2002); Watanabe (2004)]. Jami et al. (2006) in their recent paper, conducted a lattice Boltzmann prediction for natural convection in an inclined square with attached partition at one of the side walls. However, they only investigated for inclination angles 45^0 and 90^0. To the best of authors' knowledge, the investigations of the problem in hand for a wide range of inclination angles have never been conducted by the lattice Boltzmann method.

2   The Lattice Boltzmann method

In the present study, a two-dimensional case with n discrete velocities $\mathbf{c}_i\,(i = 1, ..., n)$ on a uniform, square grid was considered. There are few lattice models published in literature [Guo (2002); Zhang et. al (2005)], however, for simplicity, a nine-velocity model, $n = 9$ were considered, leading to an isotropic model as illustrated in Fig. 1.
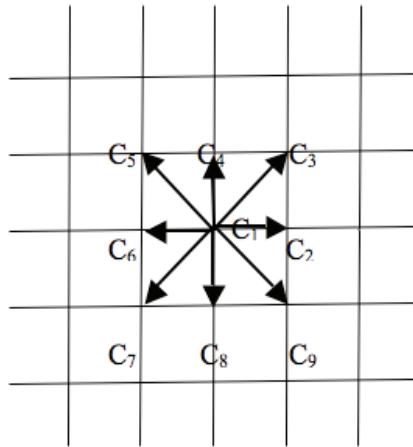
Figure 1: Two dimensional nine velocity lattice model

Instead of considering individual particles, LBM use population of particles f_i moving from a location $\mathbf{x}$ to $\mathbf{x} + \mathbf{c}_i \Delta t$ after Δt time step. In LBM, the elementary fluid flow is based on the evolution of f_i which consists of two steps: propagation and collision. These two steps can be summarized in the following equation

$$f_i\left(\mathbf{x} + \mathbf{c}_i \Delta t, t + \Delta t\right) - f_i\left(\mathbf{x}, t\right) = \Omega\left(f\right) + F_i \tag{1}$$

where $\Omega = \left.\frac{\partial f_i}{\partial t}\right|_{col}$ is an operator representing the effect of collision on particle population per unit time and F is the external force term. The most efficient way to construct the collision model has been proposed by Lallemand and Luo (2003). They indicate that particular interest is in the change in distribution function f_i in time of order τ, the average time between successive collisions. Assuming that at near equilibrium, the system is closed to a local Maxwell-Boltzmann state [Nor Azwadi and Syahrullail (2009)]. Moreover, the post-collision distribution function should be closer to equilibrium than the pre-collisions because of the H-theorem [Hou et. al (1995)]. The distribution function f_i can be related to the equilibrium

distribution function f_i^{eq} via Taylor's series expansion as follows

$$f_i^{eq}(\mathbf{x},t) \approx f_i(\mathbf{x},t) + \left.\frac{\partial f}{\partial t}\right|_{col}(\delta t) + O(\delta t)^2 \tag{2}$$

$$\left.\frac{\partial f}{\partial t}\right|_{col} = \frac{f_i^{eq}(\mathbf{x},t) - f_i(\mathbf{x},t)}{\delta t} = \frac{f_i^{eq}(\mathbf{x},t) - f_i(\mathbf{x},t)}{\tau} \tag{3}$$

where the small time interval δt has been replaced by the characteristic time between collisions τ. This model is frequently called the BGK collision model after Bhatnagar, Gross and Krook who first introduced it [Chen and Doolen (1998)]. By combining Eqns. (1) and (3), the BGK lattice Boltzmann equation can be written as

$$f_i(\mathbf{x} + \mathbf{c}_i\Delta t, t + \Delta t) - f_i(\mathbf{x},t) = \frac{f_i^{eq}(\mathbf{x},t) - f_i(\mathbf{x},t)}{\tau} + F_i \tag{4}$$

By applying the Chapmann - Enskog expansion [He and Luo (1997)], the above equations can lead to macroscopic continuity and momentum equations. However the Prandtl number obtained is fixed to a constant value [He et. al (1998)]. This is caused by the use of single relaxation time in the collision process. The relaxation time of energy carried by the particles to its equilibrium is different to that of momentum. Therefore two different relaxation times to characterize the momentum and energy transport were used. This is equivalent to introducing a new distribution function to define energy. In the present study, the internal energy density distribution function introduced by He et. al (1998) was considered as follows

$$g_i(\mathbf{x} + \mathbf{c}_i\Delta t, t + \Delta t) - g_i(\mathbf{x},t) = \frac{g_i^{eq}(\mathbf{x},t) - g_i(\mathbf{x},t)}{\tau'} \tag{5}$$

The equilibrium distributions functions of f_i^{eq} and g_i^{eq} are chosen so that they satisfy the macroscopic governing equations as follow

$$f_i^{eq} = \rho\,\omega_i\left[1 + 3\mathbf{c}_i\cdot\mathbf{u} + 4.5\,(\mathbf{c}_i\cdot\mathbf{u})^2 - 1.5\mathbf{u}^2\right] \tag{6}$$

$$g_i^{eq} = T\,\omega_i\left[1 + 3\mathbf{c}_i\cdot\mathbf{u} + 4.5\,(\mathbf{c}_i\cdot\mathbf{u})^2 - 1.5\mathbf{u}^2\right] \tag{7}$$

where ω_i is the weight function.

The macroscopic variables such as the density ρ, ?uid velocity $\boldsymbol{u}$ and temperature T can be computed in terms of the particle distribution functions as

$$\rho = \int f d\mathbf{c}$$
$$\rho\mathbf{u} = \int \mathbf{c} f d\mathbf{c} \qquad (8)$$
$$T = \int g d\mathbf{c}$$

3   Problem physics and numerical results

The physical domain of the problem is represented in Fig. 2. The conventional no-slip boundary conditions [Guo (2002)] are imposed on all the walls of the cavity. The thermal conditions applied on the left and right walls are $T(x=0,y)=T_H$ and $T(x=L,y)=T_C$. The top and bottom walls being adiabatic where $\partial T/\partial y=0$. The temperature difference between the left and right walls introduces a temperature gradient in the fluid, and the consequent density difference induces convection.
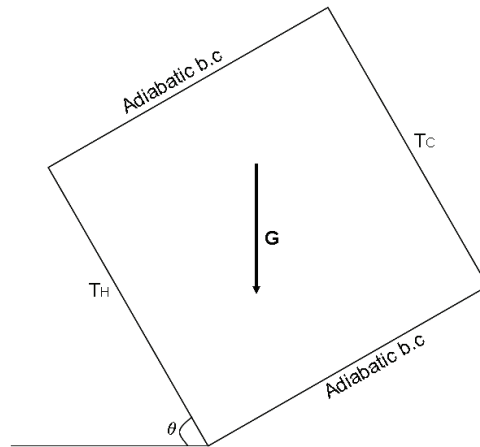
Figure 2: Physical domain of the problem

The Boussinesq approximation is applied to the buoyancy force term. With this approximation, it is assumed that all fluid properties can be considered as constant in the body force term except for the temperature dependence of the density in the gravity term. So the external force in Eq. 1 can be expressed as

$$F_i = 3\mathbf{G}(\mathbf{c}-\mathbf{u}) f_i^{eq} \qquad (9)$$

where **G** is the contribution from buoyancy force.

The dynamic similarity depends on two dimensionless parameters: the Prandtl number, *Pr* and the Rayleigh number, *Ra* defined as

$$\text{Pr} = \frac{\upsilon}{\chi} \tag{10}$$

$$Ra = \frac{g\beta\Delta T L^3}{\upsilon\chi} \tag{11}$$

where υ and χ are the fluid viscosity and thermal diffusivity, and can be related to the time relaxations in the lattice Boltzmann formulation

$$\upsilon = \frac{\tau - 1}{6} \tag{12}$$

$$\chi = \frac{\tau' - 1}{6} \tag{13}$$

The characteristic speed $v_c = \sqrt{gL\Delta T}$ was carefully chosen so that the low-Mach-number approximation is hold. Nusselt number, *Nu* is one of the most important dimensionless numbers in describing the convective transport. The average Nusselt number in the system is defined by

$$Nu = \frac{H}{\chi\Delta T} \frac{1}{H^2} \int_0^H \int_0^H q_x(x,y)\,dxdy \tag{14}$$

where $q_x(x,y) = uT(x,y) - \chi(\partial/\partial x)T(x,y)$ is the local heat flux in *x*-direction.

In all simulations, *Pr* is set at 0.71 to represent the circulation of air in the system. Through the grid dependence study, the grid sizes of 251×251 is suitable for Rayleigh numbers from 10^5 to 10^6. The convergence criterion for all the tested cases is

$$\max\left|\left((u^2+v^2)^{n+1} - (u^2+v^2)^n\right)^{\frac{1}{2}}\right| \le 10^{-7}$$
$$\max\left|T^{n+1} - T^n\right| \le 10^{-7} \tag{15}$$

where the calculation is carried out over the entire system.

For code validation, numerical investigations of natural convection in a differentially heated enclosure walls were carried out for 90^0 inclination angle. Table 1 shows the computed average Nusselt numbers in the system and comparison of the results among finite difference solutions to the Navier-Stokes equations.

Table 1: Comparison of average Nussel number

	$Ra = 10^5$	$Ra = 10^6$
Present	4.524	9.037
DQ method	4.523	8.762
Davis	4.510	8.798

The table shows our results closely agree with calculations by DQ method [Shu and Xue (1998)] and by Davis (1983) at the two values of Rayleigh number. Streamlines and isotherms predicted for flows for the three values of Rayleigh numbers and various inclination angles are shown in Figs. 3 to 8. It can be seen from the streamline plots, the liquid near the hot wall is heated and goes up due to the buoyancy effect before it hits the corner with the perfectly conducting walls and spread to a wide top wall. Then as it is cooled by the cold walls, the liquid gets heavier and goes downwards to complete the cycle.

At $Ra = 10^5$ and low value of inclination angle ($\theta = 20^0$), the central vortex appear circular in shape indicating equal magnitude of flow velocities near all four enclosure walls. The isotherms show a good mixing occurring in the center and relatively small gradient indicating small value of the local Nusselt number along the differentially heated walls. Increasing the inclination angle ($\theta = 40^0$) leads to elongated shaped of the central vortex due to higher flow velocity near the differentially heated walls. At $\theta = 60^0$, the central cell points towards the corners because of high magnitude of gravity vector drag the outer vortex along the vertical walls of the enclosure. Denser isotherms lines can be seen from the figure indicating higher values of local and average Nusselt numbers compared to the previous inclination angles. Further increasing the inclination causes the central vortex to break up into two smaller vortices. Increasing the inclination angles further results in the two vortices to grow in size indicating that some fluid from the hot or cold wall return to the same wall. For inclination angles of $\theta = 80^0$ to $\theta = 120^0$, the isotherms line are parallel to the adiabatic walls indicating that the main heat transfer mechanism is by convection. Denser isotherms lines can be seen near the bottom left and top right corners demonstrating high local Nusselt numbers near these regions. However, at higher inclination angles ($\theta \geq 140^0$), the isotherms lines are equally spaced indicating low averages Nusselt numbers in the system.

For Rayleigh number of 5×10^5 and low inclination angles, two small corner vortices appear at the top and bottom corner of the cavity indicating higher magnitude of flow velocity compared to the previous case at the same inclination angle. At angle $\theta = 60^0$, the central cells splits into three and the corner vortices disappear. The velocity boundary layer can be clearly seen for inclination angles of $\theta = 80^0$

(a) $\theta = 20^0$ (b) $\theta = 40^0$ (c) $\theta = 60^0$

(d) $\theta = 80^0$ (e) $\theta = 100^0$ (f) $\theta = 120^0$

(g) $\theta = 140^0$ (h) $\theta = 160^0$
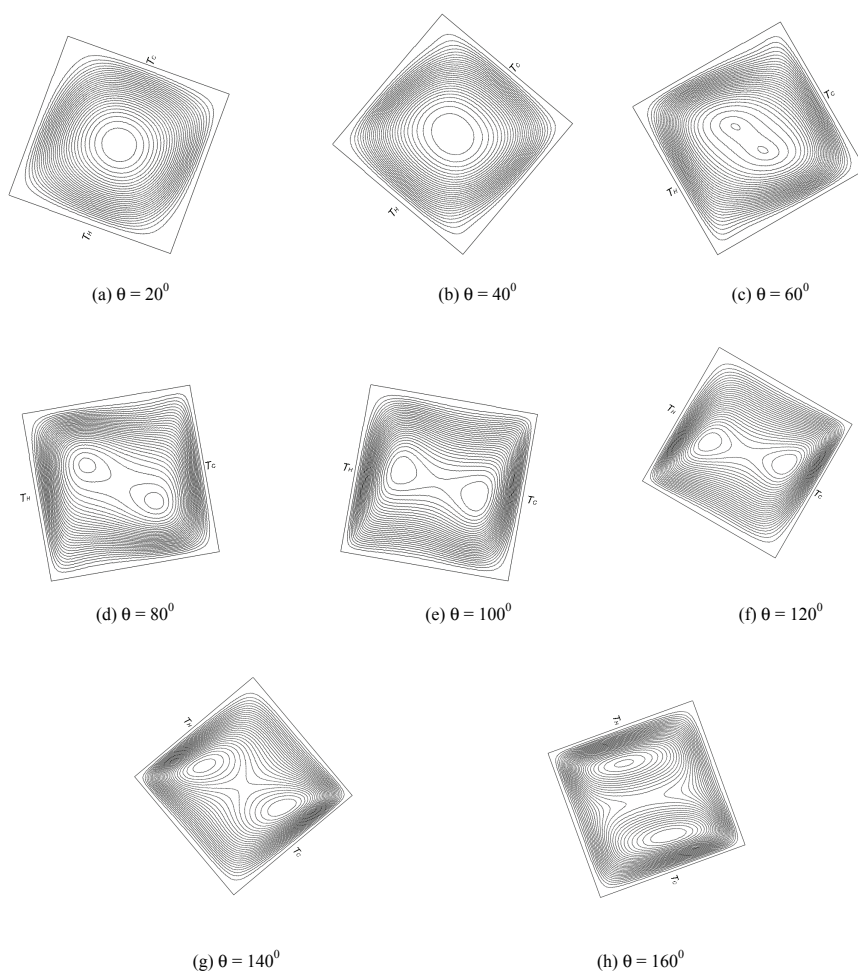
Figure 3: Plots of streamlines for Rayleigh number, $Ra = 1 \times 10^4$

and above. The isotherm patterns are similar to those for $Ra = 10^5$ at all angles. However, the thermal boundary layer are comparatively denser indicating higher local and average Nusselt numbers along the cold and hot walls.

For the simulation at the highest Rayleigh number in the present study ($Ra = 10^6$), the formation of corner vortices can be clearly seen at low inclination angles. The isotherms plots display a complex thermal behavior and good mixing of cold and hot air in the system. At inclination angle of $\theta = 60^0$, the central vortex is sepa-

(a) θ = 20⁰   (b) θ = 40⁰   (c) θ = 60⁰

(d) θ = 80⁰   (e) θ = 100⁰   (f) θ = 120⁰

(g) θ = 140⁰   (h) θ = 160⁰
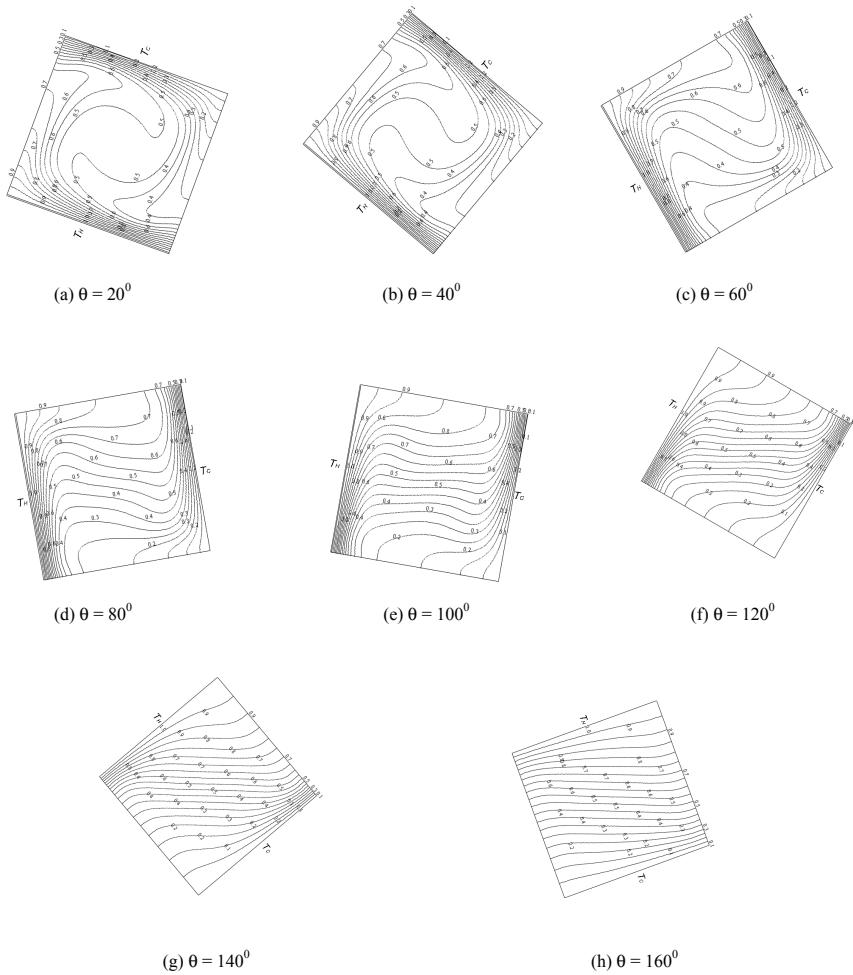
Figure 4: Plots of isotherms for Rayleigh number, $Ra = 1 \times 10^4$

rated into three smaller vortices and is vertically elongated shaped indicates relatively high flow velocity near the differentially heated walls. Most of the isotherms lines become parallel to the perfectly conducting walls indicating convection dominates the heat transfer mechanism in the system. For $\theta > 80^0$, the central vortex is stretched from corner to corner of the enclosure and is perpendicular to the gravitational vector, developed denser streamlines near these corners, indicating maximum flow velocity for the condition. On the other hand, the isotherms show similar features to those at lower Ra.

(a) θ = 20⁰   (b) θ = 40⁰   (c) θ = 60⁰

(d) θ = 80⁰   (e) θ = 100⁰   (f) θ = 120⁰

(g) θ = 140⁰   (h) θ = 160⁰
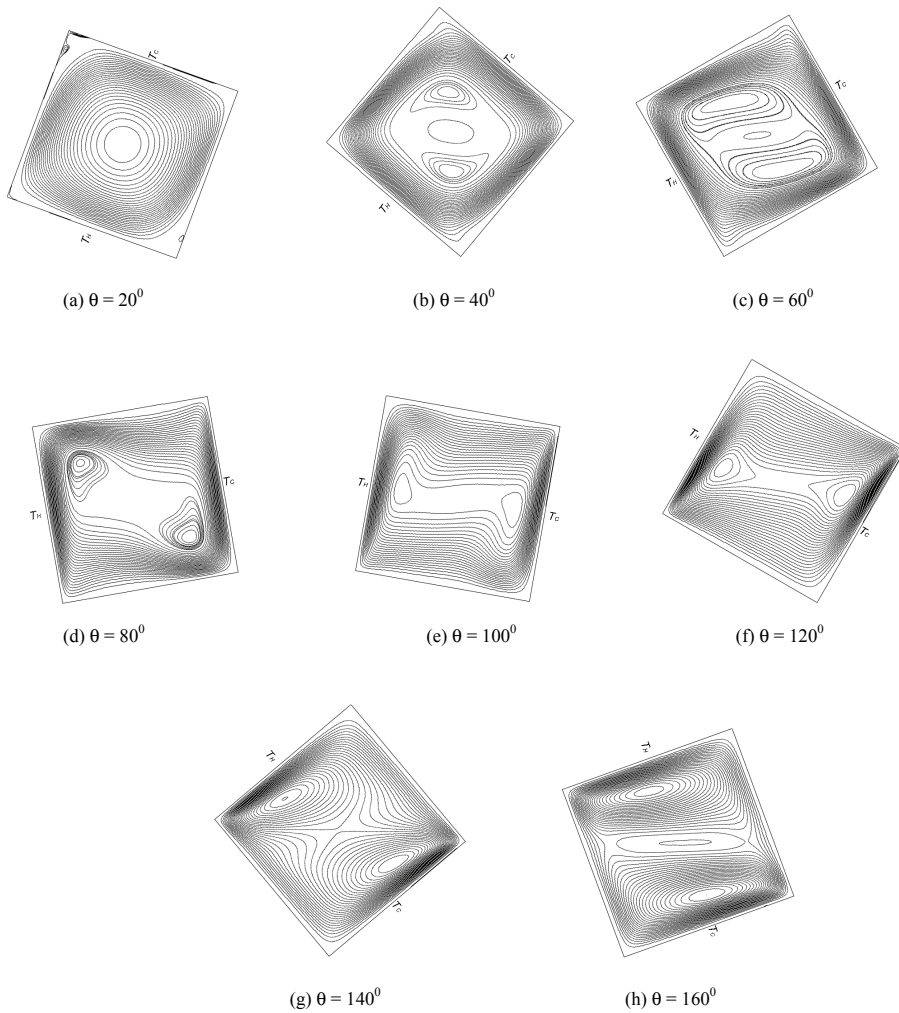
Figure 5: Plots of streamlines for Rayleigh number, $Ra = 1 \times 10^5$

The effect of the inclination angle on the average Nusselt number is shown in Fig. 9 for all values of Rayleigh numbers. One characteristic which can be observed from the figure is that; the Nusselt number increases with increasing Rayleigh number. However, the computed Nusselt numbers are lower than those for the case of perfectly conducting boundary condition [Nor Azwadi et. al (2010)] because the heat is not allowed to pass through the top and bottom walls. Interestingly, the mini-

(a) θ = 20⁰ (b) θ = 40⁰ (c) θ = 60⁰

(d) θ = 80⁰ (e) θ = 100⁰ (f) θ = 120⁰

(g) θ = 140⁰ (h) θ = 160⁰
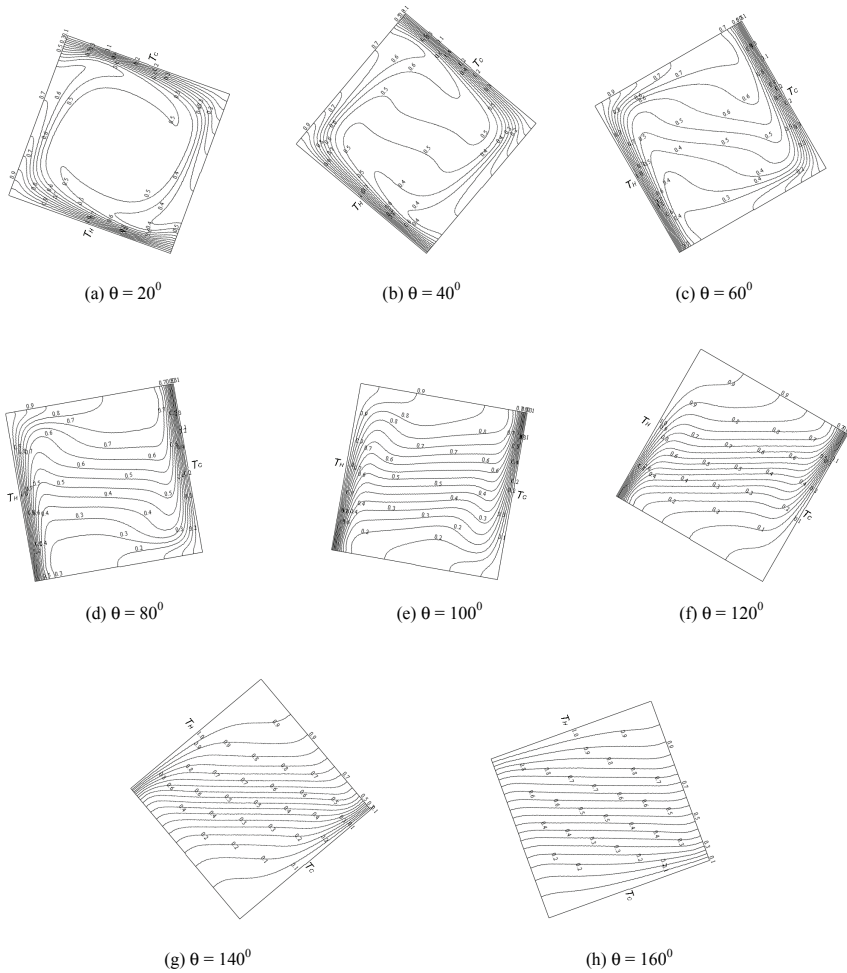
Figure 6: Plots of isotherms for Rayleigh number, $Ra = 1 \times 10^5$

mum value of the average Nusselt number is found converging to the same value and when the inclination angle approaches 180^0 for every Rayleigh number. On the other hand, the maximum value of average Nusselt number is found to be within inclination angles between $\theta = 60^0$ and $\theta = 80^0$. These can be explained by analyzing the isotherms plots which demonstrated relatively denser lines stretched along hot and cold walls leading to high temperature gradient near these regions. The figures of streamlines also demonstrate a good mixing between the hot and cool air at these inclination angles. Lower value of average Nusselt number at

(a) θ = 20⁰   (b) θ = 40⁰   (c) θ = 60⁰

(d) θ = 80⁰   (e) θ = 100⁰   (f) θ = 120⁰

(g) θ = 140⁰   (h) θ = 160⁰
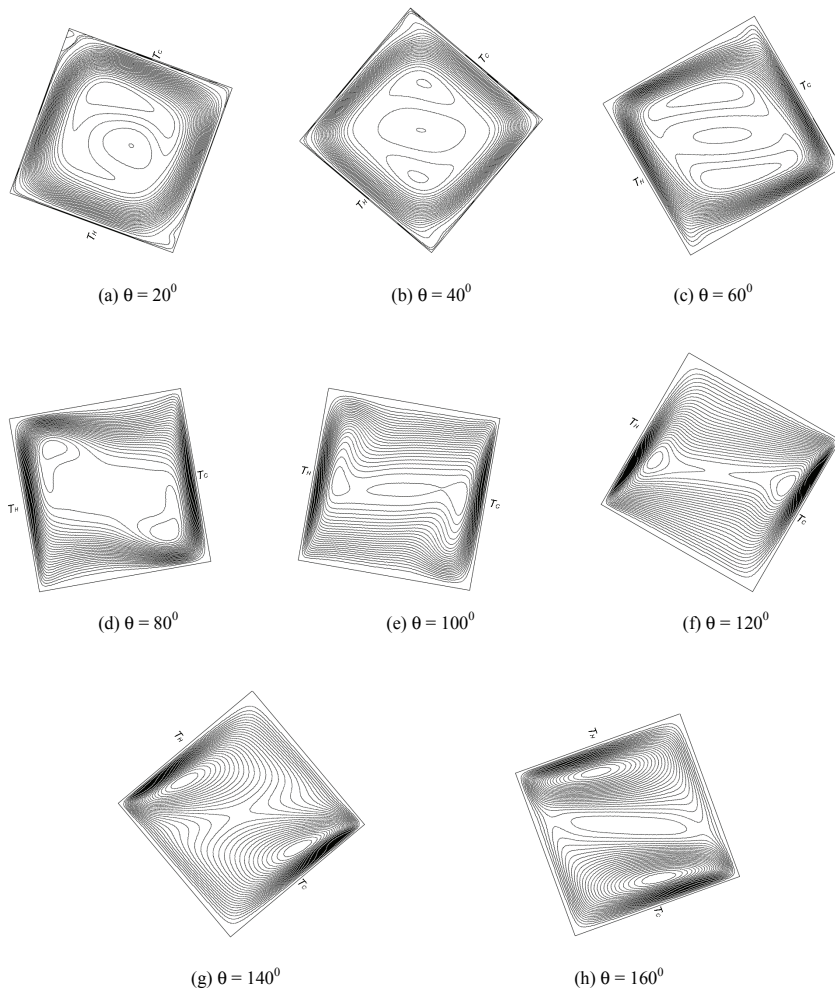
Figure 7: Plots of streamlines for Rayleigh number, $Ra = 1 \times 10^6$

lower inclination angles was due to the presence of small corner vortices which contributed smaller local heat transfer along the hot and cold walls. For the computation at higher inclination angles, where the hot wall is close to the top position, the magnitude of the gravity vector is reduced resulting in low magnitude of flow velocity along the hot wall. For this reason, the heat transfer rates are small due to the reduction in the driving potential for free convection.

(a) θ = 20^0

(b) θ = 40^0

(c) θ = 60^0

(d) θ = 80^0

(e) θ = 100^0

(f) θ = 120^0

(g) θ = 140^0

(h) θ = 160^0
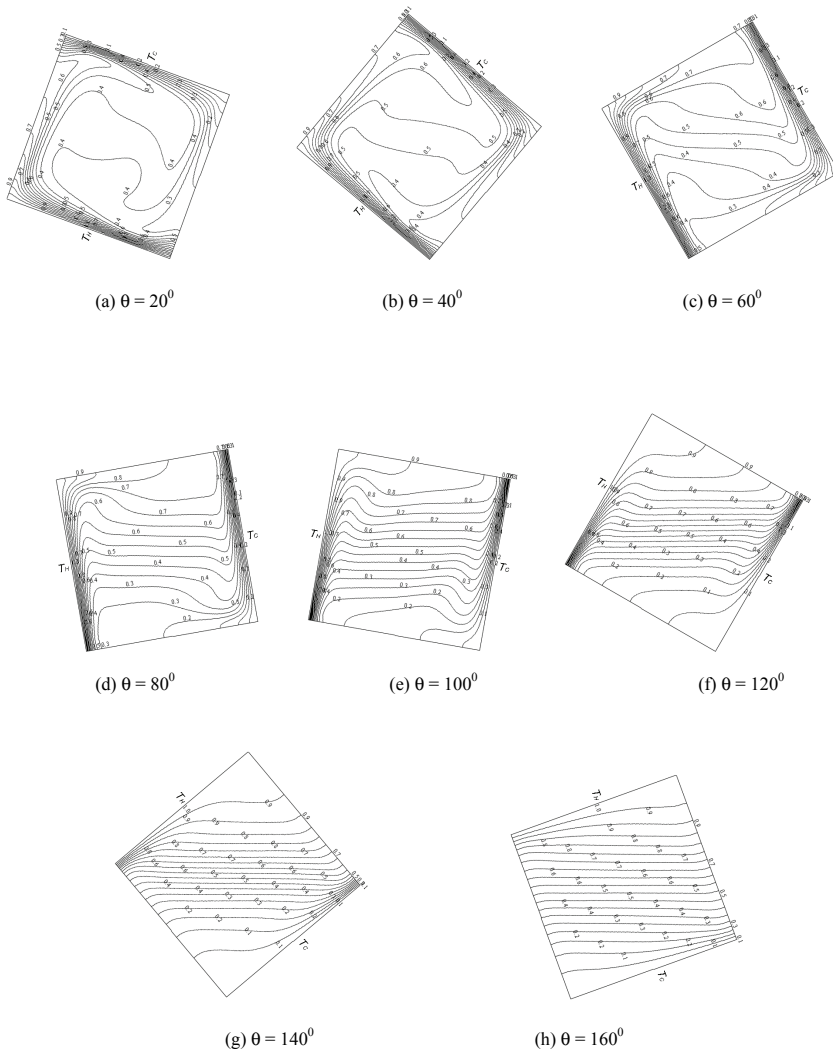
Figure 8: Plots of isotherms for Rayleigh number, $Ra = 1 \times 10^6$

4   Conclussion

The natural convection in an inclined cavity was simulated using the mesoscale numerical scheme where the Navier Stokes equation was solved indirectly using the lattice Boltzmann method. The result of streamlines plots clearly show the flow pattern and vortex structure in the cavity. The primary vortex is transformed from a
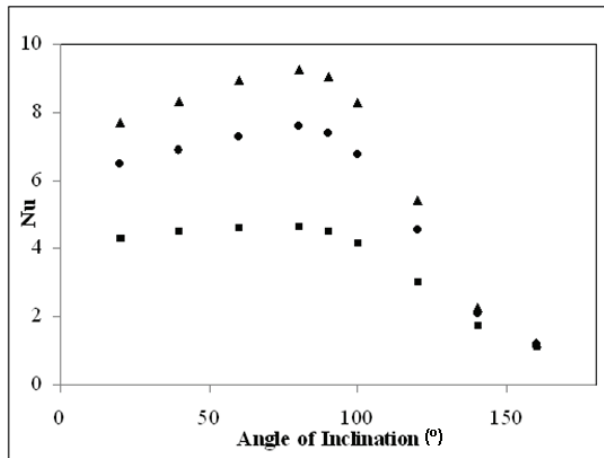
Figure 9: Plots of computed average Nusselt numbers at various wall inclination angles

single cell to triple cells as the inclination angle decreases. This work also showed that the passive-scalar thermal lattice Boltzmann model is a very efficient numerical method to study flow and heat transfer in a differentially heated inclined enclosure.

References

Chen, S.; Doolen, G. (1998): Lattice Boltzmann method for fluid flows. *Ann. Rev. Fluid Mech.*, vol. 30, pp. 329-364.

Davis, D.V. (1983): Natural convection of air in a square cavity; A benchmark numerical solution. *Intl. J. Numer. Meth. Fluids*, vol. 3, pp. 249-264.

Guo, Z. (2002): Lattice Boltzmann model for incompressible flows through porous media. *Phys. Rev. E*, vol. 66, pp. 036304/1-036304/9.

Guo, Z.; Shi, B.; Zheng, C. (2002): A coupled lattice BGK model for the Boussinesq equations. *Intl. J. Numer. Meth. Fluids*, vol. 39, pp. 325-342.

Hart, J.E. (1971): Stability of the flow in a differentially heated inclined box. *J. Fluid Mech.*, vol. 47, pp. 547-576.

He, X.; Luo, L.S. (1997): Lattice Boltzmann model for the incompressible Navier-Stokes equation. *J. Stat. Phys.*, vol. 88, pp. 927-944.

He, X.; Shan, S.; Doolen, G. (1998): A novel thermal model for lattice Boltzmann method in incompressible limit. *J. Comp. Phys.*, vol. 146, pp. 282-300.

Hou, S.; Zou, Q.; Chen, S.; Doolen, G.; Cogley, A.C. (1995): Simulation of

cavity flow by the lattice Boltzmann method. *J. Comp. Phys.*, vol. 118, pp. 329-347.

Jami, M.; Mezrhab, A.: Bouzidi, M.; Lallemand, P. (2006): Lattice-Boltzmann computation of natural convection in a partitioned enclosure with inclined partitions attached to its hot wall. *Physica A*, vol. 368, pp. 481-494.

Kuyper, R.A.; Van Der Meer, T.H., Hoogendoom, C.J.; Henkes, R.A.W.M. (1993): Numerical study of laminar and turbulent natural convection in an inclined square cavity. *Intl. J. Heat Mass Trans.*, vol. 36, pp. 2899-2911.

Lallemand, P.; Luo, L.S. (2003): Lattice Boltzmann method for moving boundaries. *J. Comp. Phys.*, vol. 184, pp. 406-421.

Nor Azwadi, C.S.; Tanahashi, T. (2006): Simplified thermal lattice Boltzmann in incompressible limit. *Intl. J. Mod. Phys. B*, vol. 21, pp. 2437-2449.

Nor Azwadi, C.S.; Tanahashi, T. (2007): Three-dimensional thermal lattice Boltzmann simulation of natural convection in a cubic cavity. *Intl. J. Mod. Phys. B*, vol. 21, pp. 87-96.

Nor Azwadi, C.S.; Syahrullail, S. (2009): A three-dimension double-population thermal lattice BGK model for simulation of natural convection heat transfer in a cubic cavity. *WSEAS Trans. Math.*, vol. 8, pp. 561-571.

Nor Azwadi, C.S.; Yasin, M.F.M.; Samion, S. (2010): Virtual study of natural convection heat transfer in an inclined square cavity, *J. App. Sci.*, vol. 10, pp. 331-336.

Ozoe, H.; Yamamoto, K.; Sayama, H.; Stuart, W.C. (1974): Natural circulation in an inclined rectangular channel heated on one side and cooled on the opposing side. *Intl. J. Heat Mass Trans.*, vol. 17, pp. 1209-1217.

Rasoul; Prinos. (1997): Natural convection in an inclined enclosure. *Intl. J. Numer. Meth. Heat Fluid Flow*, vol. 7, pp. 438-478.

Said, S.A.M.; Habib, M.A.; Badr, H.M.; Anwar, S. (2005): Turbulent natural convection between inclined isothermal plates. *Comp. Fluids*, vol. 9, pp. 1025-1039.

Shu, C.; Xue, H. (1998): Comparison of two approaches for implementing stream function boundary conditions in DQ simulation of natural convection in a square cavity. *Intl. J. Heat Fluid Flow*, vol. 19, pp. 59-68.

Tric, E.; Labrosse, G.; Betrouni, M. (2000): A first incursion into the 3D structure of natural convection of air in a differentially heated cubic cavity, from accurate numerical solutions. *Intl. J. Heat Mass Trans.*, vol. 43, pp. 4043-4056.

Watanabe, T. (2004): Flow pattern and heat transfer rate in Rayleigh Benard convection, *Phys. Fluids*, vol. 16, pp. 972-978.

Zhang, Y.; Qin, R.; Emerson, D.R. (2005): Lattice Boltzmann simulation of rarefied gas flow in microchannel. *Phys. Rev. E*, vol. 71, pp. 047702/1-047702/4.